



A precise measurement of the B^0 meson oscillation frequency

The LHCb collaboration[†]

Abstract

The oscillation frequency, Δm_d , of B^0 mesons is measured using semileptonic decays with a D^- or D^{*-} meson in the final state. The data sample corresponds to 3.0 fb^{-1} of pp collisions, collected by the LHCb experiment at centre-of-mass energies $\sqrt{s} = 7$ and 8 TeV . A combination of the two decay modes gives $\Delta m_d = (505.0 \pm 2.1 \pm 1.0) \text{ ns}^{-1}$, where the first uncertainty is statistical and the second is systematic. This is the most precise single measurement of this parameter. It is consistent with the current world average and has similar precision.

Published in Eur. Phys. J. C (2016) 76: 412.

© CERN on behalf of the LHCb collaboration, licence CC-BY-4.0.

[†]Authors are listed at the end of this paper.

1 Introduction

Flavour oscillation, or mixing, of neutral meson systems gives mass eigenstates that are different from flavour eigenstates. In the $B^0\text{--}\bar{B}^0$ system, the mass difference between mass eigenstates, Δm_d , is directly related to the square of the product of the CKM matrix elements V_{tb} and V_{td}^* , and is therefore sensitive to fundamental parameters of the Standard Model, as well as to non-perturbative strong-interaction effects and the square of the top quark mass [1]. Measurements of mixing of neutral B mesons were published for the first time by UA1 [2] and ARGUS [3]. Measurements of $B^0\text{--}\bar{B}^0$ mixing have been performed by CLEO [4], experiments at LEP and SLC [5], experiments at the Tevatron [6, 7], the B Factories experiments [8, 9] and, most recently, at LHCb [10–12]. The combined world average value for the mass difference, $\Delta m_d = (510 \pm 3) \text{ ns}^{-1}$, has a relative precision of 0.6% [13]. This paper reports a measurement of Δm_d based on $B^0 \rightarrow D^-\mu^+\nu_\mu X$ and $B^0 \rightarrow D^{*-}\mu^+\nu_\mu X$ decays,¹ where X indicates any additional particles that are not reconstructed. The data sample used for this measurement was collected at LHCb during LHC Run 1 at $\sqrt{s} = 7(8) \text{ TeV}$ in 2011 (2012), corresponding to integrated luminosities of 1.0 (2.0) fb^{-1} .

The relatively high branching fraction for semileptonic decays of B^0 mesons, along with the highly efficient lepton identification and flavour tagging capabilities at LHCb, results in abundant samples of $B^0 \rightarrow D^{(*)-}\mu^+\nu_\mu X$ decays, where the flavour of the B^0 meson at the time of production and decay can be inferred. In addition, the decay time t of B^0 mesons can be determined with adequate resolution, even though the decay is not fully reconstructed, because of the potential presence of undetected particles. It is therefore possible to precisely measure Δm_d as the frequency of matter-antimatter oscillations in a time-dependent analysis of the decay rates of unmixed and mixed events,

$$\begin{aligned} N^{\text{unmix}}(t) &\equiv N(B^0 \rightarrow D^{(*)-}\mu^+\nu_\mu X)(t) \propto e^{-\Gamma_d t} [1 + \cos(\Delta m_d t)] , \\ N^{\text{mix}}(t) &\equiv N(B^0 \rightarrow \bar{B}^0 \rightarrow D^{(*)+}\mu^-\bar{\nu}_\mu X)(t) \propto e^{-\Gamma_d t} [1 - \cos(\Delta m_d t)] , \end{aligned} \quad (1)$$

where the state assignment is based on the flavours of the B^0 meson at production and decay, which may be the same (unmixed) or opposite (mixed). In Eqn. 1, $\Gamma_d = 1/\tau_{B^0}$ is the decay width of the B^0 meson, τ_{B^0} being its lifetime. Also, in Eqn. 1 the difference in the decay widths of the mass eigenstates, $\Delta\Gamma_d$, and CP violation in mixing are neglected, due to their negligible impact on the results. The flavour asymmetry between unmixed and mixed events is

$$A(t) = \frac{N^{\text{unmix}}(t) - N^{\text{mix}}(t)}{N^{\text{unmix}}(t) + N^{\text{mix}}(t)} = \cos(\Delta m_d t) . \quad (2)$$

A description of the LHCb detector and the datasets used in this measurement is given in Sec. 2. Section 3 presents the selection criteria, the flavour tagging algorithms, and the method chosen to reconstruct the B^0 decay time. The fitting strategy and results are described in Sec. 4. A summary of the systematic uncertainties is given in Sec. 5, and conclusions are reported in Sec. 6.

¹The inclusion of charge-conjugate processes is implied throughout.

2 Detector and simulation

The LHCb detector [14,15] is a single-arm forward spectrometer covering the pseudorapidity range $2 < \eta < 5$, designed for the study of particles containing b or c quarks. The detector includes a high-precision tracking system consisting of a silicon-strip vertex detector surrounding the pp interaction region, a large-area silicon-strip detector located upstream of a dipole magnet with a bending power of about 4 Tm, and three stations of silicon-strip detectors and straw drift tubes placed downstream of the magnet. The tracking system provides a measurement of momentum, p , of charged particles with a relative uncertainty that varies from 0.5% at low momentum to 1.0% at 200 GeV/ c . The minimum distance of a track to a primary vertex (PV), the impact parameter (IP), is measured with a resolution of $(15 + 29/p_T) \mu\text{m}$, where p_T is the component of the momentum transverse to the beam, in GeV/ c . Different types of charged hadrons are distinguished using information from two ring-imaging Cherenkov (RICH) detectors. Photons, electrons and hadrons are identified by a calorimeter system consisting of scintillating-pad and preshower detectors, an electromagnetic calorimeter and a hadronic calorimeter. Muons are identified by a system composed of alternating layers of iron and multiwire proportional chambers.

The online event selection is performed by a trigger [16], which consists of a hardware stage, based on information from the calorimeter and muon systems, followed by a software stage, which applies a full event reconstruction. Candidate events are first required to pass the hardware trigger, which selects muons with a transverse momentum $p_T > 1.48 \text{ GeV}/c$ in the 7 TeV data or $p_T > 1.76 \text{ GeV}/c$ in the 8 TeV data. The software trigger requires a two-, three- or four-track secondary vertex, where one of the tracks is identified as a muon, with a significant displacement from the primary pp interaction vertices. At least one charged particle must have a transverse momentum $p_T > 1.7 \text{ GeV}/c$ and be inconsistent with originating from a PV. As it will be explained later, the software trigger selection introduces a bias on the Δm_d measurement, which is corrected for. A multivariate algorithm [17] is used for the identification of secondary vertices consistent with the decay of a b hadron.

The method chosen to reconstruct the B^0 decay time relies on Monte Carlo simulation. Simulation is also used to estimate the main background sources and to verify the fit model. In the simulation, pp collisions are generated using PYTHIA [18] with a specific LHCb configuration [19]. Decays of hadronic particles are described by EVTGEN [20], in which final-state radiation is generated using PHOTOS [21]. The interaction of the generated particles with the detector, and its response, are implemented using the GEANT4 toolkit [22] as described in Ref. [23]. Large samples of mixtures of semileptonic decays resulting in a D^- or a D^{*-} meson in the final state were simulated and the assumptions used to build these samples are assessed in the evaluation of systematic uncertainties.

3 Event selection

For charged particles used to reconstruct signal candidates, requirements are imposed on track quality, momentum, transverse momentum, and impact parameter with respect to

any PV. Tracks are required to be identified as muons, kaons or pions. The charm mesons are reconstructed through the $D^- \rightarrow K^+\pi^-\pi^-$ decay, or through the $D^{*-} \rightarrow \bar{D}^0\pi^-$, $\bar{D}^0 \rightarrow K^+\pi^-$ decay chain. The masses of the reconstructed D^- and \bar{D}^0 mesons should be within $70 \text{ MeV}/c^2$ and $40 \text{ MeV}/c^2$ of their known values [13], while the mass difference between the reconstructed D^{*-} and \bar{D}^0 mesons should lie between $140 \text{ MeV}/c^2$ and $155 \text{ MeV}/c^2$. For D^- and \bar{D}^0 candidates, the scalar sum of the p_T of the daughter tracks should be above $1800 \text{ MeV}/c$. A good quality vertex fit is required for the D^- , \bar{D}^0 , and D^{*-} candidates, and for the $D^{(*)-}\mu^+$ combinations. When more than one combination is found in an event, the one with the smallest vertex χ^2 (hereafter referred to as the B candidate) is chosen. The reconstructed vertices of D^- , \bar{D}^0 , and B candidates are required to be significantly displaced from their associated PV, where the associated PV is that which has the smallest χ^2 increase when adding the candidate. For D^- and \bar{D}^0 candidates, a large IP with respect to the associated PV is required in order to suppress charm mesons promptly produced in pp collisions. The momentum of the B candidate, and its flight direction measured using the PV and the B vertex positions, are required to be aligned. These selection criteria reduce to the per-mille level or lower the contribution of $D^{(*)-}$ decays where the charmed meson originates from the PV. The invariant mass of the B candidate is required to be in the range $[3.0, 5.2] \text{ GeV}/c^2$.

Backgrounds from $B \rightarrow J/\psi X$ decays, where one of the muons from the $J/\psi \rightarrow \mu^+\mu^-$ decay is correctly identified and the other misidentified as a pion and used to reconstruct a $D^{(*)-}$, are suppressed by applying a veto around the J/ψ mass. Similarly, a veto around the Λ_c^+ mass is applied to suppress semileptonic decays of the Λ_b^0 baryon, in which the proton of the subsequent Λ_c^+ decay into $pK^-\pi^+$ is misidentified as a pion.

The dominant background is due to $B^+ \rightarrow D^{(*)-}\mu^+\nu_\mu X$ decays, where additional particles coming from the decay of higher charm resonances, or from multi-body decays of B^+ mesons, are neglected. The fractions of B^+ decays in the D^- and D^{*-} samples are expected to be 13% and 10%, based on the branching fractions of signal and background, with uncertainties at the 10% level. This background is reduced by using a multivariate discriminant based on a boosted decision tree (BDT) algorithm [24, 25], which exploits information on the B candidate, kinematics of the higher charm resonances and isolation criteria for tracks and composite candidates in the B decay chain. Training of the BDT classifier is carried out using simulation samples of $B^0 \rightarrow D^{*-}\mu^+\nu_\mu X$ signal and $B^+ \rightarrow D^{*-}\mu^+\nu_\mu X$ background. The variables used as input for the BDT classifier are described in the Appendix. Only candidates with BDT output larger than -0.12 (-0.16) are selected in the 2011 (2012) data sample for the $B^0 \rightarrow D^-\mu^+\nu_\mu X$ mode. The BDT output is required to be larger than -0.3 in both 2011 and 2012 data samples for the $B^0 \rightarrow D^{*-}\mu^+\nu_\mu X$ mode. The impact of this requirement on signal efficiency and background retention can be seen in Fig. 3. The background from B^+ decays is reduced by 70% in both modes. Combinatorial background is evaluated by using reconstructed candidates in the $D^{(*)-}$ signal mass sidebands. Backgrounds due to decays of B_s^0 and Λ_b^0 into similar final states to those of the signal are studied through simulations.

The decay time of the B^0 meson is calculated as $t = (M_{B^0} \cdot L)/(p_{\text{rec}} \cdot c/k)$, where M_{B^0} is the mass of the B^0 , taken from Ref. [13], L is the measured decay length and p_{rec} is the

magnitude of the visible momentum, measured from the $D^{(*)-}$ meson and the muon. The correction factor k is determined from simulation by dividing the visible B^0 momentum by its true value and taking the average, $k = \langle p_{\text{rec}}/p_{\text{true}} \rangle$. This correction represents the dominant source of uncertainty in the determination of the decay time of the B^0 meson for $t > 1.5$ ps. Since the k -factor depends strongly on the decay kinematics, it is parametrised by a fourth-order polynomial as a function of the visible mass of the B^0 candidate as explained in the Appendix.

The B^0 flavour at production is determined by using information from the other b hadron present in the event. The decision of flavour tagging algorithms [26] based on the charge of leptons, kaons and of an inclusively reconstructed detached vertex, is used for the $B^0 \rightarrow D^{*-}\mu^+\nu_\mu X$ channel. In the $B^0 \rightarrow D^-\mu^+\nu_\mu X$ channel, which is subject to a larger B^+ background contamination, the decision of the tagging algorithm based on the detached vertex is excluded in order to avoid spurious background asymmetries. The statistical uncertainty on Δm_d decreases as $\mathcal{T}^{-1/2}$ where the tagging power is defined as $\mathcal{T} = \varepsilon_{\text{tag}}(1 - 2\omega)^2$, where ε_{tag} is the tagging efficiency and ω is the mistag rate. To increase the statistical precision, the events are grouped into four tagging categories of increasing predicted mistag probability η , defined by $\eta \in [0, 0.25]$, $[0.25, 0.33]$, $[0.33, 0.41]$, $[0.41, 0.47]$. The mistag probability η is evaluated for each B candidate from event and taggers properties and was calibrated on data using control samples [26]. The average mistag rates for signal and background are taken as free parameters when fitting for Δm_d . The combined tagging power [26] for the $B^0 \rightarrow D^-\mu^+\nu_\mu X$ mode is $(2.38 \pm 0.05)\%$ and $(2.46 \pm 0.04)\%$ in 2011 and 2012. For the $B^0 \rightarrow D^{*-}\mu^+\nu_\mu X$ mode, the tagging power in 2011 and 2012 is $(2.55 \pm 0.07)\%$ and $(2.32 \pm 0.04)\%$.

4 Fit strategy and results

The fit proceeds as follows. First, $D^{(*)-}$ mesons originating from semileptonic B^0 or B^+ decays are separated from the background coming from combinations of tracks not associated to a charm meson decay, by a fit to the invariant mass distributions of the selected candidates. This fit assigns to each event a covariance-weighted quantity *sWeight*, which is used in the subsequent fits to subtract statistically the contribution of the background by means of the *sPlot* procedure [27]. Then, the contribution of $D^{(*)-}$ from B^+ decays is determined in a fit to the distributions of the BDT classifier output weighted by signal *sWeights*. Next, a cut is applied on the BDT output in order to suppress the B^+ background, the mass distributions are fitted again, and new *sWeights* are determined. Finally, the oscillation frequency Δm_d is determined by a fit to the decay time distribution of unmixed and mixed candidates, weighted for the signal *sWeights* determined in the previous step.

An extended binned maximum likelihood fit to the data distributions is performed for each stage, simultaneously for the four tagging categories defined above. Data samples collected in 2011 and 2012 are treated separately.

Figure 1 shows the results of the fits to the D^- candidate mass distributions for

$B^0 \rightarrow D^- \mu^+ \nu_\mu X$ candidates. In these fits, the distributions of D^- from B^0 and B^+ decays are summed as they are described by the same probability density function (PDF): the sum of two Gaussian functions and a Crystal Ball function [28]. The yields corresponding to the D^- peak are $(5.30 \pm 0.02) \times 10^5$ and $(1.393 \pm 0.003) \times 10^6$ in 2011 and 2012 data, respectively. The combinatorial background, which contributes typically 6% under the D^- peak, is modelled with an exponential distribution.

For the $B^0 \rightarrow D^{*-} \mu^+ \nu_\mu X$ samples, a simultaneous fit to the distributions of the $K^+ \pi^-$ invariant mass, $m_{K^+ \pi^-}$, and the invariant mass difference of $K^+ \pi^- \pi^-$ and $K^+ \pi^-$ combinations, $\delta m = m_{K^+ \pi^- \pi^-} - m_{K^+ \pi^-}$, is performed. Three different components are considered: the signal D^* from B^0 or B^+ decays and two background sources. The PDF for the mass distributions of D^* from B decays is defined by the sum of two Gaussian functions and a Crystal Ball function in the $m_{K^+ \pi^-}$ mass projection and by two Gaussian functions and a Johnson function [29] in the δm mass projection. Background candidates containing a \bar{D}^0 originating from a b hadron decay without an intermediate D^* resonance, which contribute about 15% in the full δm mass range, are described by the same distribution as that of the signal for $m_{K^+ \pi^-}$, and by an empirical function based on a phase-space distribution for δm . A combinatorial background component which contributes typically 0.8% under the D^* peak is modelled with an exponential distribution for $m_{K^+ \pi^-}$ and the same empirical distribution for δm as used for the \bar{D}^0 background. All parameters that describe signal and background shapes are allowed to vary freely in the invariant mass fits. The results of the 2011 and 2012 fits for these parameters are compatible within the statistical uncertainties. Figure 2 shows the results of the fit to the $B^0 \rightarrow D^{*-} \mu^+ \nu_\mu X$ samples, projected onto the two mass observables. The yields corresponding to the D^* peak are $(2.514 \pm 0.006) \times 10^5$ and $(5.776 \pm 0.009) \times 10^5$ in 2011 and 2012 data.

The fraction of B^+ background in data, α_{B^+} , is determined with good precision by fitting the distribution of the BDT classifier, where templates for signal and B^+ background are obtained from simulation. Fits are performed separately in tagging categories for 2011 and 2012 data, giving fractions of B^+ of 6% and 3% on average for the $B^0 \rightarrow D^- \mu^+ \nu_\mu X$ and the $B^0 \rightarrow D^{*-} \mu^+ \nu_\mu X$ modes with relative variation of the order of 10% between samples. The results of the fits to 2012 data for both modes are given in Fig. 3. Limited knowledge of the exclusive decays used to build the simulation templates leads to systematic uncertainties of 0.5% and 0.4% on the B^+ fractions for $B^0 \rightarrow D^- \mu^+ \nu_\mu X$ and $B^0 \rightarrow D^{*-} \mu^+ \nu_\mu X$. In the decay time fit, the B^+ fractions are kept fixed. The statistical and systematic uncertainties on α_{B^+} lead to a systematic uncertainty on Δm_d , which is reported in Sec. 5.

The oscillation frequency Δm_d is determined from a binned maximum likelihood fit to the distribution of the B^0 decay time t of candidates classified as mixed ($q = -1$) or unmixed ($q = 1$) according to the flavour of the B^0 meson at production and decay time.

The total PDF for the fit is given by

$$\mathcal{P}(t, q) = \mathcal{S}(t, q) + \alpha_{B^+} \mathcal{B}^+(t, q), \quad (3)$$

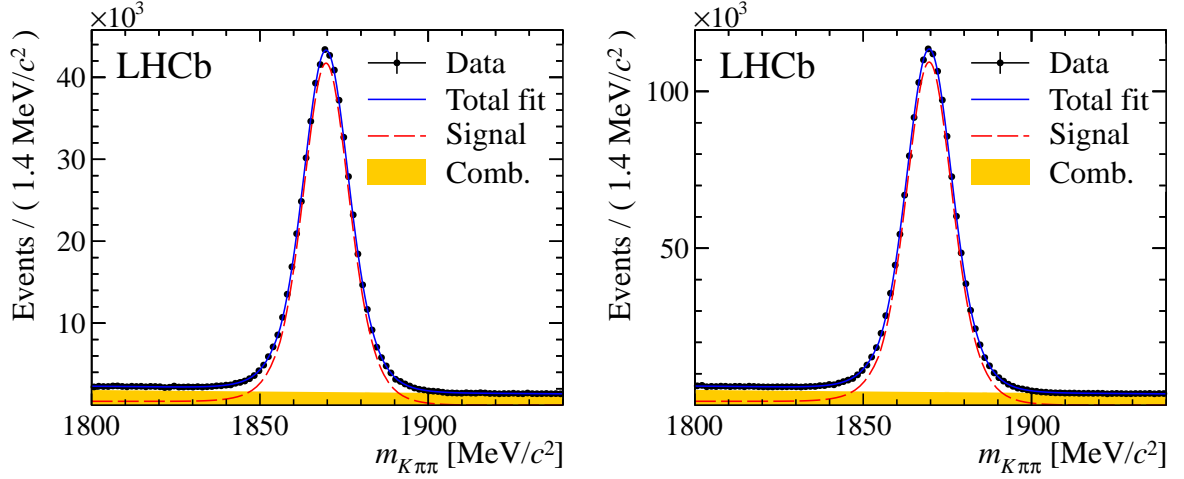


Figure 1: Distribution of $m_{K\pi\pi}$ for the $B^0 \rightarrow D^- \mu^+ \nu_\mu X$ candidates in (left) 2011 and (right) 2012 data. Projections of the fit function are superimposed (blue continuous line) for the full PDF and its components: (red dashed line) signal D^- from B^0 or B^+ decays and (filled yellow area) combinatorial background.

where the time distributions for signal and background are given by

$$\begin{aligned} \mathcal{S}(t, q) &= \mathcal{N} e^{-\Gamma_d t} \left(1 + q(1 - 2\omega_{\text{sig}}) \cos \Delta m_d t \right), \\ \mathcal{B}^+(t, q) &= \mathcal{N}_{B^+} e^{-\Gamma_u t} \left(\frac{1+q}{2} - q\omega_{B^+} \right). \end{aligned} \quad (4)$$

Here \mathcal{N} and \mathcal{N}_{B^+} are normalisation factors, and Γ_d and Γ_u are fixed in the fit to their world average values [13], where $\Gamma_u = 1/\tau_{B^+}$, with τ_{B^+} being the lifetime of the B^+ meson. The mistag fractions for signal and B^+ components, ω_{sig} and ω_{B^+} , vary freely in the fit. To account for the time resolution, both distributions in Eq. 4 are convolved with a resolution model that takes into account uncertainties on both the decay length and the momentum. The distributions used in the fit are therefore obtained by a double convolution. The contribution accounting for the decay length resolution is described by a triple Gaussian function with an effective width corresponding to a time resolution of 75 fs, as determined from simulation. The contribution accounting for the uncertainty on the momentum is described by the distribution of $p_{\text{rec}}/(k \cdot p_{\text{true}})$, obtained from the simulation. This second convolution is dominant above 1.5 ps. Finally, the function \mathcal{P} is multiplied by an acceptance function $a(t)$ to account for the effect of the trigger and offline selection and reconstruction. The acceptance is described by a sum of cubic spline polynomials [30], which may be different for signal and B^+ background. The ratios between spline coefficients of the B^+ background acceptance and those of the signal acceptance are fixed to the values predicted by simulation. The spline coefficients for signal are then determined for each tagging category directly from the tagged time-dependent fit to data.

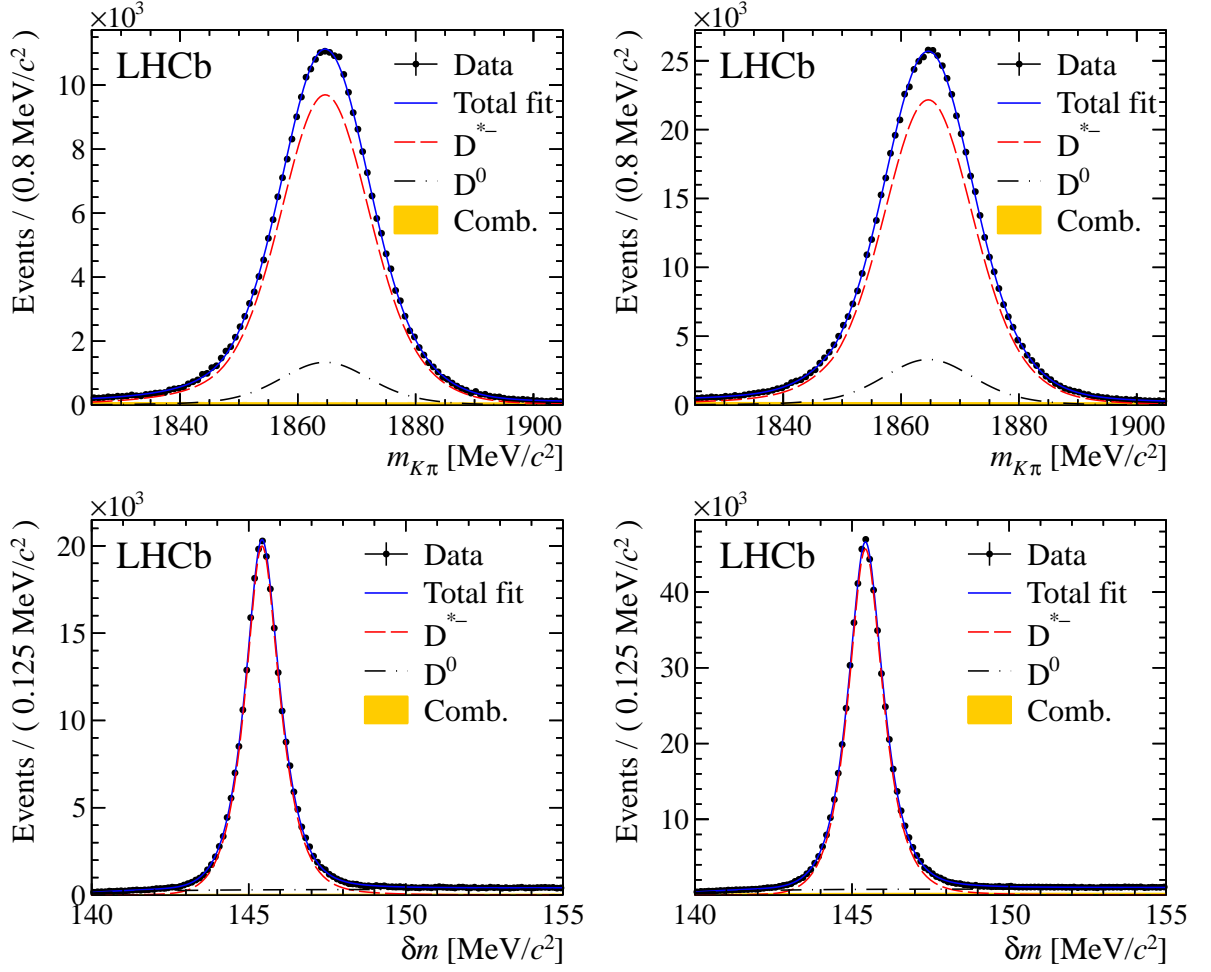


Figure 2: Distributions of (top) $m_{K\pi}$ and (bottom) δm for $B^0 \rightarrow D^{*-} \mu^+ \nu_\mu X$ candidates in (left) 2011 and (right) 2012 data. Projections of the fit function are superimposed for (blue continuous line) the full PDF and its components: (red dashed line) signal D^{*-} from B^0 or B^+ decays, (black dashed-dotted line) \bar{D}^0 from B and (filled yellow area) combinatorial backgrounds.

The fitting strategy is validated with simulation. A bias is observed in the Δm_d value, due to a correlation between the decay time and its resolution, which is not taken into account when parameterizing the signal shape. Simulation shows that this correlation is introduced by the requirements of the software trigger and offline selection on the impact parameters of D^- and \bar{D}^0 with respect to the PV. Values for this bias, of up to 4 ns^{-1} with a 10% uncertainty, are determined for each mode and for each year by fitting the true and corrected time distributions and taking the differences between the resulting values of Δm_d . The uncertainty on the bias is treated as a systematic uncertainty on Δm_d .

The values of Δm_d , obtained from the time-dependent fit and corrected for the fit bias, are reported in Table 1. Systematic uncertainties are discussed below. The four

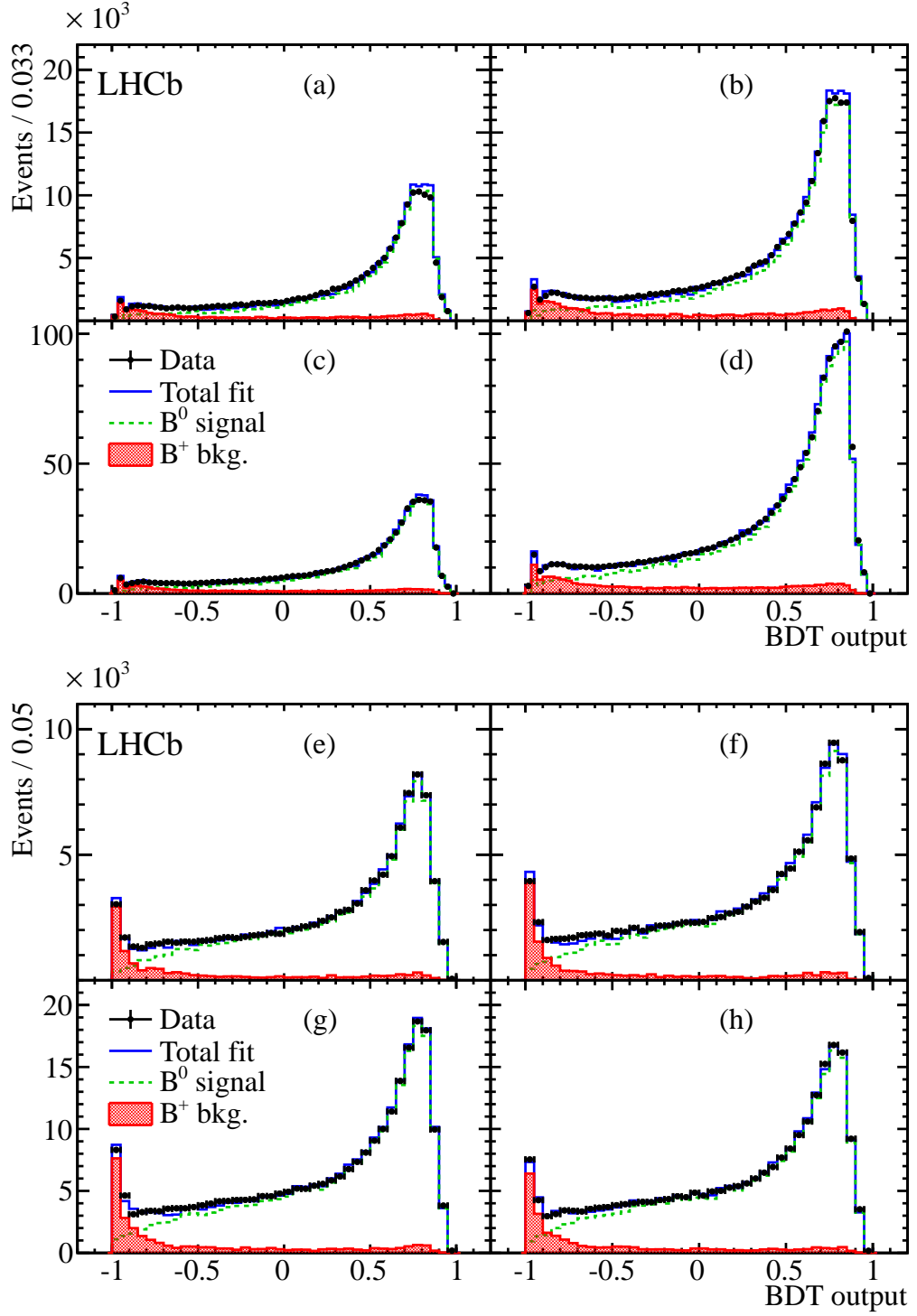


Figure 3: Fits to the output of the B^+ veto BDT for (top four plots) $B^0 \rightarrow D^-\mu^+\nu_\mu X$ and (bottom four plots) $B^+ \rightarrow D^{*-}\mu^+\nu_\mu X$ in 2012 data, for each tagging category. The filled red histogram, the dashed green line, and the continuous blue line correspond to background, signal, and total templates, respectively. The average mistag fraction per category increases when going from (a) to (d), and (e) to (h).

Table 1: Results for Δm_d measured in each mode for 2011 and 2012 data separately, for the total sample, and for the combination of the two modes. The quoted uncertainties for the separate samples are statistical only. For the total samples and the combination, they refer to statistical and total systematic uncertainties, respectively.

Mode	2011 sample Δm_d [ns ⁻¹]	2012 sample Δm_d [ns ⁻¹]	Total sample Δm_d [ns ⁻¹]
$B^0 \rightarrow D^- \mu^+ \nu_\mu X$	506.2 ± 5.1	505.2 ± 3.1	$505.5 \pm 2.7 \pm 1.1$
$B^0 \rightarrow D^{*-} \mu^+ \nu_\mu X$	497.5 ± 6.1	508.3 ± 4.0	$504.4 \pm 3.4 \pm 1.0$
combination	$505.0 \pm 2.1 \pm 1.0$		

independent Δm_d values are compatible within statistical uncertainties. Figure 4 shows the fit projections for the decay time distributions for the candidates in the category with lowest mistag rate in 2012 data. The time-dependent asymmetries for the $B^0 \rightarrow D^- \mu^+ \nu_\mu X$ and $B^0 \rightarrow D^{*-} \mu^+ \nu_\mu X$ modes in 2011 and 2012 data are shown in Figs. 5 and 6. Fits are also performed in subsamples of different track multiplicity, number of primary vertices, magnet polarity, run periods, and muon charges. Statistically compatible results are obtained in all cases. A combination of the two Δm_d determinations, including systematic uncertainties, is given in Sec. 6.

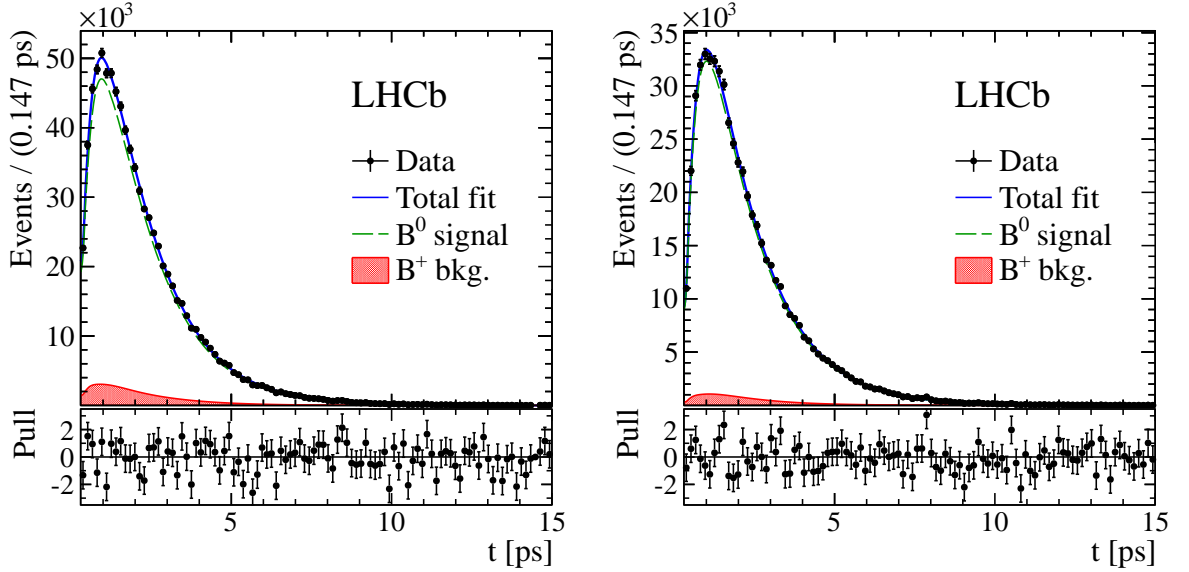


Figure 4: Decay time distributions for (left) $B^0 \rightarrow D^- \mu^+ \nu_\mu X$ and (right) $B^0 \rightarrow D^{*-} \mu^+ \nu_\mu X$ in the category with lowest mistag in 2012 data.

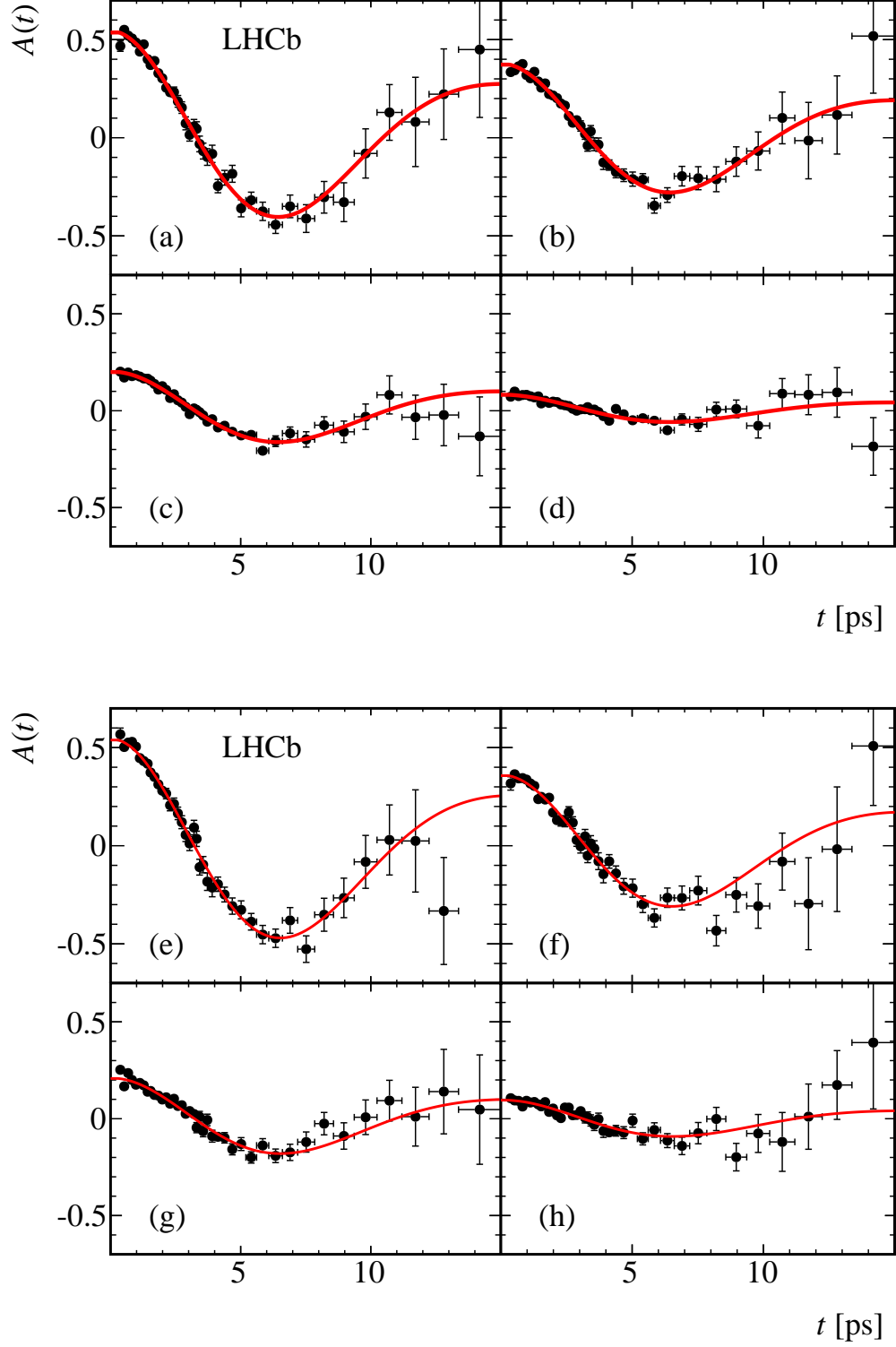


Figure 5: Mixing asymmetry projections in the four tagging categories for (top plots) $B^0 \rightarrow D^- \mu^+ \nu_\mu X$ and (bottom plots) $B^0 \rightarrow D^{*-} \mu^+ \nu_\mu X$ for 2011 data. The average mistag per category increases when going from (a) to (d), and from (e) to (h).

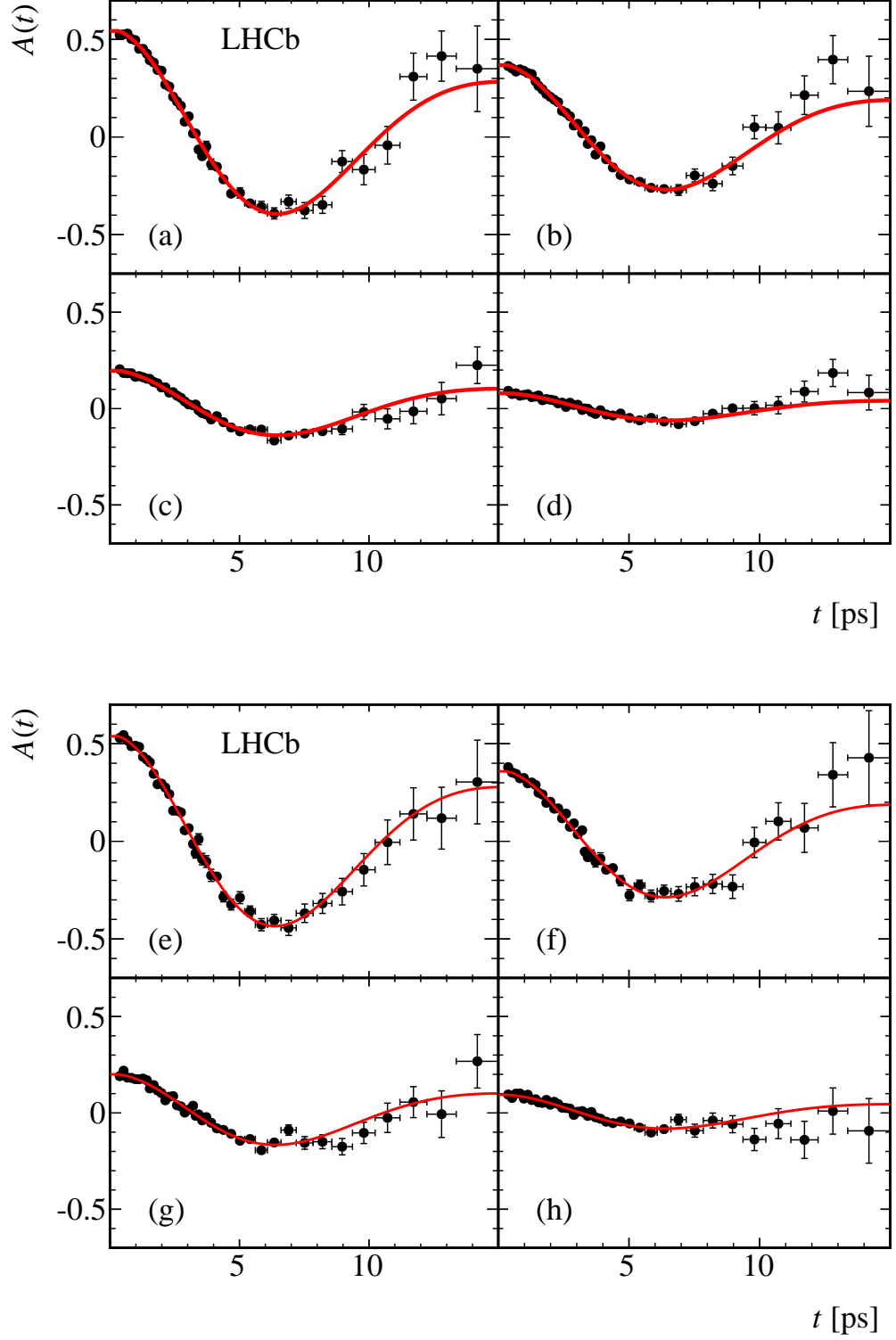


Figure 6: Mixing asymmetry projections in the four tagging categories for (top plots) $B^0 \rightarrow D^- \mu^+ \nu_\mu X$ and (bottom plots) $B^0 \rightarrow D^{*-} \mu^+ \nu_\mu X$ for 2012 data. The average mistag per category increases when going from (a) to (d), and from (e) to (h).

Table 2: Sources of systematic uncertainties on Δm_d , separated into those that are correlated and uncorrelated between the two decay channels $B^0 \rightarrow D^- \mu^+ \nu_\mu X$ and $B^0 \rightarrow D^{*-} \mu^+ \nu_\mu X$.

Source of uncertainty	$B^0 \rightarrow D^- \mu^+ \nu_\mu X$ [ns ⁻¹]		$B^0 \rightarrow D^{*-} \mu^+ \nu_\mu X$ [ns ⁻¹]	
	Uncorrelated	Correlated	Uncorrelated	Correlated
B^+ background	0.4	0.1	0.4	–
Other backgrounds	–	0.5	–	–
k -factor distribution	0.4	0.5	0.3	0.6
Other fit-related	0.5	0.4	0.3	0.5
Total	0.8	0.8	0.6	0.8

5 Systematic uncertainties

The contribution of each source of systematic uncertainty is evaluated by using a large number of parameterized simulations. The difference between the default Δm_d value and the result obtained when repeating the fits after having adjusted the inputs to those corresponding to the systematic variation under test, is taken as a systematic uncertainty. Systematic uncertainties are summarized in Table 2.

5.1 Background from B^+

The fraction of B^+ background is estimated from data with a very small statistical uncertainty. A variation, within their uncertainties, of the branching fractions of semileptonic B^0 decays resulting in a D^{*-} or D^- in the final state gives systematic uncertainties on the B^+ fractions of 0.5% and 0.4% for $B^0 \rightarrow D^- \mu^+ \nu_\mu X$ and $B^0 \rightarrow D^{*-} \mu^+ \nu_\mu X$. The resulting uncertainty on Δm_d is 0.1 ns⁻¹ in $B^0 \rightarrow D^- \mu^+ \nu_\mu X$ and is negligible for $B^0 \rightarrow D^{*-} \mu^+ \nu_\mu X$. In the default fit, the decay time acceptance ratio of the B^0 and the B^+ components is taken from simulation. The time acceptance is to a large extent due to the cut on the D^0 impact parameter. A possible systematic effect due to an incorrect determination of the acceptance ratio from simulation is estimated by fitting events, generated with the default signal and background acceptances, with an acceptance ratio determined by using a tighter D^0 IP cut than the default. This gives an uncertainty of 0.4 ns⁻¹ on both decay modes. The above systematic uncertainties are considered as uncorrelated between the two channels.

The uncertainty on Δm_d from the resolution on the B^+ decay length is 0.1 ns⁻¹ in the $B^0 \rightarrow D^- \mu^+ \nu_\mu X$ channel and is negligible in the $B^0 \rightarrow D^{*-} \mu^+ \nu_\mu X$ channel.

5.2 Other backgrounds

The impact of the knowledge of backgrounds due to semileptonic B_s^0 decays with $D^{(*)-}$ in the final state is estimated by varying their contributions within the uncertainties on their

branching fractions. This effect has a negligible impact on Δm_d for both channels. For the $B^0 \rightarrow D^- \mu^+ \nu_\mu X$ channel, there is an additional contribution from $B_s^0 \rightarrow D_s^- \mu^+ \nu_\mu$ decays, where a kaon in the $D_s^- \rightarrow K^- K^+ \pi^-$ decay is misidentified as a pion, which gives an 8% contribution due to D_s^- peaking under the D^- mass. A difference in Δm_d of 0.5 ns^{-1} is observed.

The $\Lambda_b^0 \rightarrow n D^{*-} \mu^+ \nu_\mu$ decay has not been observed. However, because of the similar final state, it can be mistaken for B^+ background, since neither of them exhibits oscillatory behaviour. Dedicated simulated samples are generated by assuming colour suppression with respect to signal, and are used to estimate a signal contamination of 0.2% from Λ_b^0 decays, with 100% uncertainty, which gives a negligible effect on Δm_d .

Small contributions from $B \rightarrow D^{(*)-} D_s^+ X$ decays, with the D_s^+ decaying semileptonically give an uncertainty of 0.2 ns^{-1} on Δm_d in the $B^0 \rightarrow D^- \mu^+ \nu_\mu X$ mode, and a negligible effect for the $B^0 \rightarrow D^{*-} \mu^+ \nu_\mu X$ mode.

5.3 The k -factor

Two main sources of systematic uncertainty are related to the k -factor. The first, due to possible differences in the B momentum spectrum between simulation and data, is studied by comparing the B momentum in $B^+ \rightarrow J/\psi K^+$ decays in data and simulation, and reweighting signal simulation to estimate the effect on the k -factor distribution and therefore on Δm_d . The systematic uncertainties on Δm_d from this effect for $B^0 \rightarrow D^- \mu^+ \nu_\mu X$ and $B^0 \rightarrow D^{*-} \mu^+ \nu_\mu X$ are 0.3 ns^{-1} and 0.5 ns^{-1} . The second source, related to the uncertainties on the measurements of the branching fractions for the exclusive modes which are used to build the simulated samples, is evaluated by varying the branching fractions of exclusive decays one at a time by one standard deviation, and reweighting the corresponding k -factor distribution. An uncertainty of 0.4 ns^{-1} is obtained for both $B^0 \rightarrow D^- \mu^+ \nu_\mu X$ and $B^0 \rightarrow D^{*-} \mu^+ \nu_\mu X$ channels. The systematic uncertainties from the k -factor correction are taken to be correlated between the two channels.

The systematic uncertainties on Δm_d from the finite number of events in the simulation sample used to compute the k -factor corrections are 0.3 and 0.4 ns^{-1} ($B^0 \rightarrow D^- \mu^+ \nu_\mu X$) and 0.2 and 0.3 ns^{-1} ($B^0 \rightarrow D^{*-} \mu^+ \nu_\mu X$) for the 2011 and 2012 samples, respectively.

5.4 Other systematic uncertainties

Possible differences between data and simulation in the resolution on the B^0 flight distance are evaluated by using the results of a study reported in Ref. [31], and scaling the widths of the triple Gaussian function by a factor 1.5 with respect to the default. Uncertainties of 0.3 ns^{-1} and 0.5 ns^{-1} on Δm_d are obtained for $B^0 \rightarrow D^- \mu^+ \nu_\mu X$ and $B^0 \rightarrow D^{*-} \mu^+ \nu_\mu X$. Both channels are affected by the same discrepancy between data and simulation; thus these systematic uncertainties are taken as correlated.

Since all parameters are allowed to vary freely in the invariant mass fits, the uncertainties from the invariant mass model are small. As a cross-check, when the fits are repeated using the $sWeights$ determined without splitting the mass fits in tagging categories, negligible

variation in Δm_d is found. Signal and background mistag probabilities are free parameters in the fit, and therefore no systematic uncertainty is associated to them.

Asymmetries in the production of neutral and charged B mesons, in tagging efficiency and mistag probabilities, and in the reconstruction of the final state are neglected in the Δm_d fits. Also, the B^0 semileptonic CP asymmetry a_{sl}^d is assumed to be zero. The systematic uncertainty on Δm_d arising from these assumptions is studied using parameterized simulations with the asymmetries set to zero, to their measured values, and to random variations from their central values within the uncertainties [32]. The resulting uncertainty on Δm_d is found to be negligible.

The bias in Δm_d from the correlation between the decay time and its resolution is determined using the simulation. The dependence of Δm_d on possible differences between data and simulation has already been considered above by varying the composition of the simulation sample used to construct the k -factor distribution. Since the bias is related to the cut on the D meson IP with respect to the PV, the fits are repeated with a k -factor distribution obtained with a tighter cut on the IP, and the difference with respect to the default is taken as the systematic uncertainty. The systematic uncertainties (0.5 and 0.3 ns^{-1} for $B^0 \rightarrow D^- \mu^+ \nu_\mu X$ and $B^0 \rightarrow D^{*-} \mu^+ \nu_\mu X$, respectively) related to the bias are considered as uncorrelated between the channels, as they are determined from different simulation samples and the time-biasing cuts, responsible for the systematic uncertainty on the bias, are different for the two channels.

The knowledge of the length scale of the LHCb experiment is limited by the uncertainties from the metrology measurements of the silicon-strip vertex detector. This was evaluated in the context of the Δm_s measurement and found to be 0.022% [31]. This translates into an uncertainty on Δm_d of 0.1 ns^{-1} . The uncertainty on the knowledge of the momentum scale is determined by reconstructing the masses of various particles and is found to be 0.03% [33]. This uncertainty results in a 0.2 ns^{-1} uncertainty in Δm_d in both modes. Both uncertainties are considered correlated across the two channels.

Effects due to the choice of the binning scheme and fitting ranges are found to be negligible.

6 Summary and conclusion

A combined value of Δm_d is obtained as a weighted average of the four measurements performed in $B^0 \rightarrow D^- \mu^+ \nu_\mu X$ and $B^0 \rightarrow D^{*-} \mu^+ \nu_\mu X$ in the years 2011 and 2012. First, the 2011 and 2012 results for each decay mode are averaged according to their statistical uncertainties. The combined results are shown in the last column of Table 1. Then, the resulting Δm_d values of each mode are averaged taking account of statistical and uncorrelated systematic uncertainties. The correlated systematic uncertainty is added in quadrature to the resulting uncertainty. The combined result is shown in the last row of Table 1.

In conclusion, the oscillation frequency, Δm_d , in the $B^0-\bar{B}^0$ system is measured in semileptonic B^0 decays using data collected in 2011 and 2012 at LHCb. The decays

$B^0 \rightarrow D^- \mu^+ \nu_\mu X$ and $B^0 \rightarrow D^{*-} \mu^+ \nu_\mu X$ are used, where the D mesons are reconstructed in Cabibbo-favoured decays $D^- \rightarrow K^+ \pi^- \pi^-$ and $D^{*-} \rightarrow \bar{D}^0 \pi^-$, with $\bar{D}^0 \rightarrow K^+ \pi^-$. A combined Δm_d measurement is obtained,

$$\Delta m_d = (505.0 \pm 2.1 \text{ (stat)} \pm 1.0 \text{ (syst)}) \text{ ns}^{-1},$$

which is compatible with previous LHCb results and the world average [13]. This is the most precise single measurement of this quantity, with a total uncertainty similar to the current world average.

Acknowledgements

We express our gratitude to our colleagues in the CERN accelerator departments for the excellent performance of the LHC. We thank the technical and administrative staff at the LHCb institutes. We acknowledge support from CERN and from the national agencies: CAPES, CNPq, FAPERJ and FINEP (Brazil); NSFC (China); CNRS/IN2P3 (France); BMBF, DFG and MPG (Germany); INFN (Italy); FOM and NWO (The Netherlands); MNiSW and NCN (Poland); MEN/IFA (Romania); MinES and FANO (Russia); MinECo (Spain); SNSF and SER (Switzerland); NASU (Ukraine); STFC (United Kingdom); NSF (USA). We acknowledge the computing resources that are provided by CERN, IN2P3 (France), KIT and DESY (Germany), INFN (Italy), SURF (The Netherlands), PIC (Spain), GridPP (United Kingdom), RRCKI and Yandex LLC (Russia), CSCS (Switzerland), IFIN-HH (Romania), CBPF (Brazil), PL-GRID (Poland) and OSC (USA). We are indebted to the communities behind the multiple open source software packages on which we depend. Individual groups or members have received support from AvH Foundation (Germany), EPLANET, Marie Skłodowska-Curie Actions and ERC (European Union), Conseil Général de Haute-Savoie, Labex ENIGMASS and OCEVU, Région Auvergne (France), RFBR and Yandex LLC (Russia), GVA, XuntaGal and GENCAT (Spain), Herchel Smith Fund, The Royal Society, Royal Commission for the Exhibition of 1851 and the Leverhulme Trust (United Kingdom).

A Appendix

A.1 BDT classifier

The variables used as input for the BDT classifier are the following:

- Visible mass of the B candidate, $m_B \equiv m(D^{(*)-}\mu^+)$
- Corrected mass [34], defined as $m_{\text{corr}} = \sqrt{m_B^2 + p_T(B)^2} + p_T(B)$, where $p_T(B)$ is the visible momentum of the B candidate transverse to its flight direction; the B flight direction is measured using the primary vertex and B vertex positions
- Angle between the visible momentum of the B candidate and its flight direction
- Impact parameter, $\text{IP}(\pi, D)$, with respect to the decay vertex of the D^- (\bar{D}^0), of the track with the smallest impact parameter with respect to the B candidate
- Smallest vertex χ^2 of the combination of the D^- (D^{*-}) with any other track, and the invariant mass of this combination
- Cone isolation $I = \frac{p_T(B)}{p_T(B) + \sum_i p_{T,i}}$, where the sum is computed over tracks which satisfy $\sqrt{\delta\eta_i^2 + \delta\phi_i^2} < 1$, $\delta\eta_i$ and $\delta\phi_i$ being the difference in pseudorapidity and in polar angle ϕ between the track and the B candidate
- Track isolation variables, used to discriminate tracks originating from the B vertex from those originating elsewhere:
 - Number of nearby tracks [35], computed for each track in the B decay chain
 - The output of an isolation BDT [35] estimated for the B candidate
 - A second isolation BDT, similar to the previous, which exploits a different training strategy and additional variables, computed for tracks originating from D^- (\bar{D}^0) decays, those coming from the B decay, and all tracks in the decay chain.

The TMVA package [36], used to train and test the classifier, ranks the input variables according to their discriminating power between signal and background.

A.2 Distributions of the k -factor

Figure 7 shows distributions of the k -factor as a function of the visible mass of the B candidate, as obtained with samples of simulated signal events. In each plot, the average k -factor and the result of a polynomial fit are also shown.

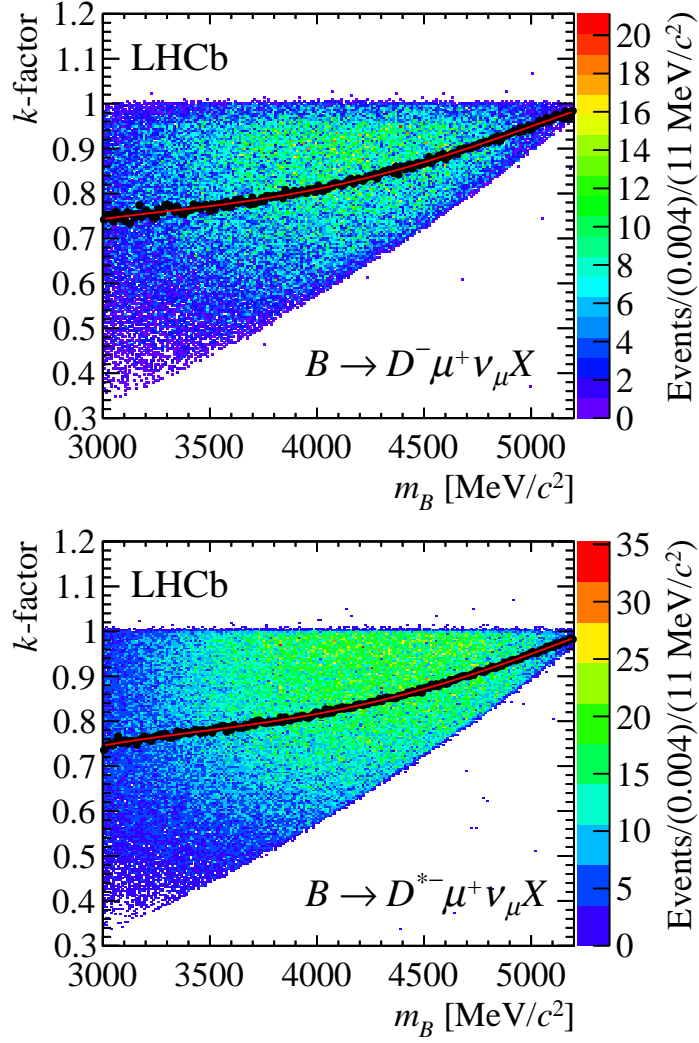


Figure 7: The k -factor distribution and the average k -factor (black points) as a function of the visible mass of the B candidate, in samples of simulated (top) $B^0 \rightarrow D^- \mu^+ \nu_\mu X$ and (bottom) $B^0 \rightarrow D^{*-} \mu^+ \nu_\mu X$ decays. Polynomial fits to the average k -factor are also shown as a solid (red) line.

References

- [1] O. Schneider, in Particle Data Group, K. A. Olive *et al.*, *Review of particle physics*, Chin. Phys. **C38** (2014) 090001, and references therein.
- [2] UA1 collaboration, C. Albajar *et al.*, *Search for $B^0 \bar{B}^0$ oscillations at the CERN proton - anti-proton collider. 2.*, Phys. Lett. **B186** (1987) 247, [Erratum: Phys. Lett. **B197** (1987) 565].
- [3] ARGUS collaboration, H. Albrecht *et al.*, *Observation of $B^0 \bar{B}^0$ mixing*, Phys. Lett. **B192** (1987) 245.
- [4] CLEO, B. H. Behrens *et al.*, *Precise measurement of $b0$ - anti- $B0$ mixing parameters at the $\text{upsilon}(4S)$* , Phys. Lett. **B490** (2000) 36, [arXiv:hep-ex/0005013](#).
- [5] ALEPH, CDF, DELPHI, L3, OPAL, SLD collaborations, D. Abbaneo *et al.*, *Combined results on B hadron production rates, lifetimes, oscillations and semileptonic decays*, [arXiv:hep-ex/0009052](#).
- [6] D0 collaboration, V. M. Abazov *et al.*, *Measurement of B_d mixing using opposite-side flavor tagging*, Phys. Rev. **D74** (2006) 112002, [arXiv:hep-ex/0609034](#).
- [7] CDF collaboration, T. Affolder *et al.*, *Measurement of the $B^0 \bar{B}^0$ oscillation frequency using $\ell^- D^{*+}$ pairs and lepton flavor tags*, Phys. Rev. **D60** (1999) 112004, [arXiv:hep-ex/9907053](#).
- [8] BaBar collaboration, B. Aubert *et al.*, *Measurement of the \bar{B}^0 lifetime and the $B^0 \bar{B}^0$ oscillation frequency using partially reconstructed $\bar{B}^0 \rightarrow D^{*+} \ell^- \bar{\nu}_\ell$ decays*, Phys. Rev. **D73** (2006) 012004, [arXiv:hep-ex/0507054](#).
- [9] Belle collaboration, K. Abe *et al.*, *Improved measurement of CP -violation parameters $\sin 2\phi_1$ and $|\lambda|$, B meson lifetimes, and $B^0 - \bar{B}^0$ mixing parameter Δm_d* , Phys. Rev. **D71** (2005) 072003, [arXiv:hep-ex/0408111](#), [Erratum: Phys. Rev. **D71**, 079903 (2005)].
- [10] LHCb collaboration, R. Aaij *et al.*, *Measurement of the $B_s^0 - \bar{B}_s^0$ oscillation frequency Δm_s in $B_s^0 \rightarrow D_s^-(3)\pi$ decays*, Phys. Lett. **B709** (2012) 177, [arXiv:1112.4311](#).
- [11] LHCb collaboration, R. Aaij *et al.*, *Observation of $B_s^0 - \bar{B}_s^0$ mixing and measurement of mixing frequencies using semileptonic B decays*, Eur. Phys. J. **C73** (2013) 2655, [arXiv:1308.1302](#).
- [12] LHCb collaboration, R. Aaij *et al.*, *Measurement of the $B^0 \bar{B}^0$ oscillation frequency Δm_d with the decays $B^0 \rightarrow D^- \pi^+$ and $B^0 \rightarrow J/\psi K^{*0}$* , Phys. Lett. **B719** (2013) 318, [arXiv:1210.6750](#).

- [13] Particle Data Group, K. A. Olive *et al.*, *Review of particle physics*, Chin. Phys. **C38** (2014) 090001.
- [14] LHCb collaboration, A. A. Alves Jr. *et al.*, *The LHCb detector at the LHC*, JINST **3** (2008) S08005.
- [15] LHCb collaboration, R. Aaij *et al.*, *LHCb detector performance*, Int. J. Mod. Phys. **A30** (2015) 1530022, [arXiv:1412.6352](#).
- [16] A. Puig, *The LHCb trigger in 2011 and 2012*, LHCb-PUB-2014-046.
- [17] V. V. Gligorov and M. Williams, *Efficient, reliable and fast high-level triggering using a bonsai boosted decision tree*, JINST **8** (2013) P02013, [arXiv:1210.6861](#).
- [18] T. Sjöstrand, S. Mrenna, and P. Skands, *PYTHIA 6.4 physics and manual*, JHEP **05** (2006) 026, [arXiv:hep-ph/0603175](#); T. Sjöstrand, S. Mrenna, and P. Skands, *A brief introduction to PYTHIA 8.1*, Comput. Phys. Commun. **178** (2008) 852, [arXiv:0710.3820](#).
- [19] I. Belyaev *et al.*, *Handling of the generation of primary events in Gauss, the LHCb simulation framework*, J. Phys. Conf. Ser. **331** (2011) 032047.
- [20] D. J. Lange, *The EvtGen particle decay simulation package*, Nucl. Instrum. Meth. **A462** (2001) 152.
- [21] P. Golonka and Z. Was, *PHOTOS Monte Carlo: A precision tool for QED corrections in Z and W decays*, Eur. Phys. J. **C45** (2006) 97, [arXiv:hep-ph/0506026](#).
- [22] Geant4 collaboration, J. Allison *et al.*, *Geant4 developments and applications*, IEEE Trans. Nucl. Sci. **53** (2006) 270; Geant4 collaboration, S. Agostinelli *et al.*, *Geant4: A simulation toolkit*, Nucl. Instrum. Meth. **A506** (2003) 250.
- [23] M. Clemencic *et al.*, *The LHCb simulation application, Gauss: Design, evolution and experience*, J. Phys. Conf. Ser. **331** (2011) 032023.
- [24] L. Breiman, J. H. Friedman, R. A. Olshen, and C. J. Stone, *Classification and regression trees*, Wadsworth international group, Belmont, California, USA, 1984.
- [25] R. E. Schapire and Y. Freund, *A decision-theoretic generalization of on-line learning and an application to boosting*, J. Comput. Syst. Sci. **55** (1997) 119.
- [26] LHCb collaboration, R. Aaij *et al.*, *Opposite-side flavour tagging of B mesons at the LHCb experiment*, Eur. Phys. J. **C72** (2012) 2022, [arXiv:1202.4979](#).
- [27] M. Pivk and F. R. Le Diberder, *sPlot: A statistical tool to unfold data distributions*, Nucl. Instrum. Meth. **A555** (2005) 356, [arXiv:physics/0402083](#).

- [28] T. Skwarnicki, *A study of the radiative cascade transitions between the Upsilon-prime and Upsilon resonances*, PhD thesis, Institute of Nuclear Physics, Krakow, 1986, DESY-F31-86-02.
- [29] N. L. Johnson, *Systems of frequency curves generated by methods of translation*, Biometrika **36** (1949) 149.
- [30] C. de Boor, *A Practical Guide to Splines (revised edition)*, Springer, New York, NY, USA, 2001.
- [31] LHCb collaboration, R. Aaij *et al.*, *Precision measurement of the B_s^0 - \bar{B}_s^0 oscillation frequency in the decay $B_s^0 \rightarrow D_s^- \pi^+$* , New J. Phys. **15** (2013) 053021, [arXiv:1304.4741](#).
- [32] LHCb collaboration, R. Aaij *et al.*, *Measurement of the semileptonic CP asymmetry in B^0 - \bar{B}^0 mixing*, Phys. Rev. Lett. **114** (2015) 041601, [arXiv:1409.8586](#).
- [33] LHCb collaboration, R. Aaij *et al.*, *Precision measurement of D meson mass differences*, JHEP **06** (2013) 065, [arXiv:1304.6865](#).
- [34] SLD collaboration, K. Abe *et al.*, *A measurement of R_b using a vertex mass tag*, Phys. Rev. Lett. **80** (1998) 660, [arXiv:hep-ex/9708015](#).
- [35] LHCb collaboration, R. Aaij *et al.*, *Search for the lepton flavour violating decay $\tau^- \rightarrow \mu^- \mu^+ \mu^-$* , JHEP **02** (2015) 121, [arXiv:1409.8548](#).
- [36] P. Speckmayer, A. Hocker, J. Stelzer, and H. Voss, *The toolkit for multivariate data analysis, TMVA 4*, J. Phys. Conf. Ser. **219** (2010) 032057.

LHCb collaboration

R. Aaij³⁹, C. Abellán Beteta⁴¹, B. Adeva³⁸, M. Adinolfi⁴⁷, A. Affolder⁵³, Z. Ajaltouni⁵, S. Akar⁶, J. Albrecht¹⁰, F. Alessio³⁹, M. Alexander⁵², S. Ali⁴², G. Alkhazov³¹, P. Alvarez Cartelle⁵⁴, A.A. Alves Jr⁵⁸, S. Amato², S. Amerio²³, Y. Amhis⁷, L. An³, L. Anderlini¹⁸, J. Anderson⁴¹, G. Andreassi⁴⁰, M. Andreotti^{17,f}, J.E. Andrews⁵⁹, R.B. Appleby⁵⁵, O. Aquines Gutierrez¹¹, F. Archilli³⁹, P. d'Argent¹², A. Artamonov³⁶, M. Artuso⁶⁰, E. Aslanides⁶, G. Auriemma^{26,m}, M. Baalouch⁵, S. Bachmann¹², J.J. Back⁴⁹, A. Badalov³⁷, C. Baesso⁶¹, W. Baldini^{17,39}, R.J. Barlow⁵⁵, C. Barschel³⁹, S. Barsuk⁷, W. Barter³⁹, V. Batozskaya²⁹, V. Battista⁴⁰, A. Bay⁴⁰, L. Beaucourt⁴, J. Beddow⁵², F. Bedeschi²⁴, I. Bediaga¹, L.J. Bel⁴², V. Bellec⁴⁰, N. Belloli^{21,j}, I. Belyaev³², E. Ben-Haim⁸, G. Bencivenni¹⁹, S. Benson³⁹, J. Benton⁴⁷, A. Berezchnoy³³, R. Bernet⁴¹, A. Bertolin²³, M.-O. Bettler³⁹, M. van Beuzekom⁴², A. Bien¹², S. Bifani⁴⁶, P. Billoir⁸, T. Bird⁵⁵, A. Birnkraut¹⁰, A. Bizzeti^{18,h}, T. Blake⁴⁹, F. Blanc⁴⁰, J. Blouw¹¹, S. Blusk⁶⁰, V. Bocci²⁶, A. Bondar³⁵, N. Bondar^{31,39}, W. Bonivento¹⁶, S. Borghi⁵⁵, M. Borsato⁷, T.J.V. Bowcock⁵³, E. Bowen⁴¹, C. Bozzi¹⁷, S. Braun¹², M. Britsch¹¹, T. Britton⁶⁰, J. Brodzicka⁵⁵, N.H. Brook⁴⁷, E. Buchanan⁴⁷, A. Bursche⁴¹, J. Buytaert³⁹, S. Cadeddu¹⁶, R. Calabrese^{17,f}, M. Calvi^{21,j}, M. Calvo Gomez^{37,o}, P. Campana¹⁹, D. Campora Perez³⁹, L. Capriotti⁵⁵, A. Carbone^{15,d}, G. Carboni^{25,k}, R. Cardinale^{20,i}, A. Cardini¹⁶, P. Carniti^{21,j}, L. Carson⁵¹, K. Carvalho Akiba^{2,39}, G. Casse⁵³, L. Cassina^{21,j}, L. Castillo Garcia⁴⁰, M. Cattaneo³⁹, Ch. Cauet¹⁰, G. Cavallero²⁰, R. Cenci^{24,s}, M. Charles⁸, Ph. Charpentier³⁹, M. Chefdeville⁴, S. Chen⁵⁵, S.-F. Cheung⁵⁶, N. Chiapolini⁴¹, M. Chrzasczcz⁴¹, X. Cid Vidal³⁹, G. Ciezarek⁴², P.E.L. Clarke⁵¹, M. Clemencic³⁹, H.V. Cliff⁴⁸, J. Closier³⁹, V. Coco³⁹, J. Cogan⁶, E. Cogneras⁵, V. Cogoni^{16,e}, L. Cojocariu³⁰, G. Collazuol^{23,q}, P. Collins³⁹, A. Comerma-Montells¹², A. Contu^{16,39}, A. Cook⁴⁷, M. Coombes⁴⁷, S. Coquereau⁸, G. Corti³⁹, M. Corvo^{17,f}, B. Couturier³⁹, G.A. Cowan⁵¹, D.C. Craik⁴⁹, A. Crocombe⁴⁹, M. Cruz Torres⁶¹, S. Cunliffe⁵⁴, R. Currie⁵⁴, C. D'Ambrosio³⁹, E. Dall'Occo⁴², J. Dalseno⁴⁷, P.N.Y. David⁴², A. Davis⁵⁸, O. De Aguiar Francisco², K. De Bruyn⁶, S. De Capua⁵⁵, M. De Cian¹², J.M. De Miranda¹, L. De Paula², P. De Simone¹⁹, C.-T. Dean⁵², D. Decamp⁴, M. Deckenhoff¹⁰, L. Del Buono⁸, N. Déléage⁴, M. Demmer¹⁰, D. Derkach⁶⁶, O. Deschamps⁵, F. Dettori³⁹, B. Dey²², A. Di Canto³⁹, F. Di Ruscio²⁵, H. Dijkstra³⁹, S. Donleavy⁵³, F. Dordei¹², M. Dorigo⁴⁰, A. Dosil Suárez³⁸, D. Dossett⁴⁹, A. Dovbnya⁴⁴, K. Dreimanis⁵³, L. Dufour⁴², G. Dujany⁵⁵, F. Dupertuis⁴⁰, P. Durante³⁹, R. Dzhelyadin³⁶, A. Dziurda²⁷, A. Dzyuba³¹, S. Easo^{50,39}, U. Egede⁵⁴, V. Egorychev³², S. Eidelman³⁵, S. Eisenhardt⁵¹, U. Eitschberger¹⁰, R. Ekelhof¹⁰, L. Eklund⁵², I. El Rifai⁵, Ch. Elsasser⁴¹, S. Ely⁶⁰, S. Esen¹², H.M. Evans⁴⁸, T. Evans⁵⁶, A. Falabella¹⁵, C. Färber³⁹, N. Farley⁴⁶, S. Farry⁵³, R. Fay⁵³, D. Ferguson⁵¹, V. Fernandez Albor³⁸, F. Ferrari¹⁵, F. Ferreira Rodrigues¹, M. Ferro-Luzzi³⁹, S. Filippov³⁴, M. Fiore^{17,39,f}, M. Fiorini^{17,f}, M. Firlej²⁸, C. Fitzpatrick⁴⁰, T. Fiutowski²⁸, K. Fohl³⁹, P. Fol⁵⁴, M. Fontana¹⁶, F. Fontanelli^{20,i}, D. C. Forshaw⁶⁰, R. Forty³⁹, M. Frank³⁹, C. Frei³⁹, M. Frosini¹⁸, J. Fu²², E. Furfaro^{25,k}, A. Gallas Torreira³⁸, D. Galli^{15,d}, S. Gallorini^{23,39}, S. Gambetta⁵¹, M. Gandelman², P. Gandini⁵⁶, Y. Gao³, J. García Pardiñas³⁸, J. Garra Tico⁴⁸, L. Garrido³⁷, D. Gascon³⁷, C. Gaspar³⁹, R. Gauld⁵⁶, L. Gavardi¹⁰, G. Gazzoni⁵, D. Gerick¹², E. Gersabeck¹², M. Gersabeck⁵⁵, T. Gershon⁴⁹, Ph. Ghez⁴, S. Gian⁴⁰, V. Gibson⁴⁸, O.G. Girard⁴⁰, L. Giubega³⁰, V.V. Gligorov³⁹, C. Göbel⁶¹, D. Golubkov³², A. Golutvin^{54,32,39}, A. Gomes^{1,a}, C. Gotti^{21,j}, M. Grabalosa Gándara⁵, R. Graciani Diaz³⁷, L.A. Granado Cardoso³⁹, E. Graugés³⁷, E. Graverini⁴¹, G. Graziani¹⁸, A. Greco³⁰, E. Greening⁵⁶, S. Gregson⁴⁸, P. Griffith⁴⁶, L. Grillo¹², O. Grünberg⁶⁴, B. Gui⁶⁰, E. Gushchin³⁴, Yu. Guz^{36,39}, T. Gys³⁹, T. Hadavizadeh⁵⁶,

C. Hadjivasiliou⁶⁰, G. Haefeli⁴⁰, C. Haen³⁹, S.C. Haines⁴⁸, S. Hall⁵⁴, B. Hamilton⁵⁹, X. Han¹²,
 S. Hansmann-Menzemer¹², N. Harnew⁵⁶, S.T. Harnew⁴⁷, J. Harrison⁵⁵, J. He³⁹, T. Head⁴⁰,
 V. Heijne⁴², A. Heister⁹, K. Hennessy⁵³, P. Henrard⁵, L. Henry⁸, J.A. Hernando Morata³⁸,
 E. van Herwijnen³⁹, M. Heß⁶⁴, A. Hicheur², D. Hill⁵⁶, M. Hoballah⁵, C. Hombach⁵⁵,
 W. Hulsbergen⁴², T. Humair⁵⁴, N. Hussain⁵⁶, D. Hutchcroft⁵³, D. Hynds⁵², M. Idzik²⁸,
 P. Ilten⁵⁷, R. Jacobsson³⁹, A. Jaeger¹², J. Jalocha⁵⁶, E. Jans⁴², A. Jawahery⁵⁹, F. Jing³,
 M. John⁵⁶, D. Johnson³⁹, C.R. Jones⁴⁸, C. Joram³⁹, B. Jost³⁹, N. Jurik⁶⁰, S. Kandybei⁴⁴,
 W. Kanso⁶, M. Karacson³⁹, T.M. Karbach^{39,†}, S. Karodia⁵², M. Kecke¹², M. Kelsey⁶⁰,
 I.R. Kenyon⁴⁶, M. Kenzie³⁹, T. Ketel⁴³, B. Khanji^{21,39,j}, C. Khurewathanakul⁴⁰, T. Kirn⁹,
 S. Klaver⁵⁵, K. Klimaszewski²⁹, O. Kochebina⁷, M. Kolpin¹², I. Komarov⁴⁰, R.F. Koopman⁴³,
 P. Koppenburg^{42,39}, M. Kozeiha⁵, L. Kravchuk³⁴, K. Kreplin¹², M. Kreps⁴⁹, G. Krocker¹²,
 P. Krokovny³⁵, F. Kruse¹⁰, W. Krzemien²⁹, W. Kucewicz^{27,n}, M. Kucharczyk²⁷,
 V. Kudryavtsev³⁵, A. K. Kuonen⁴⁰, K. Kurek²⁹, T. Kvaratskheliya³², D. Lacarrere³⁹,
 G. Lafferty⁵⁵, A. Lai¹⁶, D. Lambert⁵¹, G. Lanfranchi¹⁹, C. Langenbruch⁴⁹, B. Langhans³⁹,
 T. Latham⁴⁹, C. Lazzeroni⁴⁶, R. Le Gac⁶, J. van Leerdam⁴², J.-P. Lees⁴, R. Lefèvre⁵,
 A. Leflat^{33,39}, J. Lefrançois⁷, E. Lemos Cid³⁸, O. Leroy⁶, T. Lesiak²⁷, B. Leverington¹², Y. Li⁷,
 T. Likhomanenko^{66,65}, M. Liles⁵³, R. Lindner³⁹, C. Linn³⁹, F. Lionetto⁴¹, B. Liu¹⁶, X. Liu³,
 D. Loh⁴⁹, I. Longstaff⁵², J.H. Lopes², D. Lucchesi^{23,q}, M. Lucio Martinez³⁸, H. Luo⁵¹,
 A. Lupato²³, E. Luppi^{17,f}, O. Lupton⁵⁶, N. Lusardi²², A. Lusiani²⁴, F. Machefert⁷, F. Maciuc³⁰,
 O. Maev³¹, K. Maguire⁵⁵, S. Malde⁵⁶, A. Malinin⁶⁵, G. Manca⁷, G. Mancinelli⁶, P. Manning⁶⁰,
 A. Mapelli³⁹, J. Maratas⁵, J.F. Marchand⁴, U. Marconi¹⁵, C. Marin Benito³⁷, P. Marino^{24,39,s},
 J. Marks¹², G. Martellotti²⁶, M. Martin⁶, M. Martinelli⁴⁰, D. Martinez Santos³⁸,
 F. Martinez Vidal⁶⁷, D. Martins Tostes², A. Massafferri¹, R. Matev³⁹, A. Mathad⁴⁹, Z. Mathe³⁹,
 C. Matteuzzi²¹, A. Mauri⁴¹, B. Maurin⁴⁰, A. Mazurov⁴⁶, M. McCann⁵⁴, J. McCarthy⁴⁶,
 A. McNab⁵⁵, R. McNulty¹³, B. Meadows⁵⁸, F. Meier¹⁰, M. Meissner¹², D. Melnychuk²⁹,
 M. Merk⁴², E. Michielin²³, D.A. Milanes⁶³, M.-N. Minard⁴, D.S. Mitzel¹², J. Molina Rodriguez⁶¹,
 I.A. Monroy⁶³, S. Monteil⁵, M. Morandin²³, P. Morawski²⁸, A. Morda⁶, M.J. Morello^{24,s},
 J. Moron²⁸, A.B. Morris⁵¹, R. Mountain⁶⁰, F. Muheim⁵¹, D. Müller⁵⁵, J. Müller¹⁰, K. Müller⁴¹,
 V. Müller¹⁰, M. Mussini¹⁵, B. Muster⁴⁰, P. Naik⁴⁷, T. Nakada⁴⁰, R. Nandakumar⁵⁰, A. Nandi⁵⁶,
 I. Nasteva², M. Needham⁵¹, N. Neri²², S. Neubert¹², N. Neufeld³⁹, M. Neuner¹², A.D. Nguyen⁴⁰,
 T.D. Nguyen⁴⁰, C. Nguyen-Mau^{40,p}, V. Niess⁵, R. Niet¹⁰, N. Nikitin³³, T. Nikodem¹²,
 A. Novoselov³⁶, D.P. O'Hanlon⁴⁹, A. Oblakowska-Mucha²⁸, V. Obraztsov³⁶, S. Ogilvy⁵²,
 O. Okhrimenko⁴⁵, R. Oldeman^{16,e}, C.J.G. Onderwater⁶⁸, B. Osorio Rodrigues¹,
 J.M. Otalora Goicochea², A. Otto³⁹, P. Owen⁵⁴, A. Oyanguren⁶⁷, A. Palano^{14,c}, F. Palombo^{22,t},
 M. Palutan¹⁹, J. Panman³⁹, A. Papanestis⁵⁰, M. Pappagallo⁵², L.L. Pappalardo^{17,f},
 C. Pappenheimer⁵⁸, C. Parkes⁵⁵, G. Passaleva¹⁸, G.D. Patel⁵³, M. Patel⁵⁴, C. Patrignani^{20,i},
 A. Pearce^{55,50}, A. Pellegrino⁴², G. Penso^{26,l}, M. Pepe Altarelli³⁹, S. Perazzini^{15,d}, P. Perret⁵,
 L. Pescatore⁴⁶, K. Petridis⁴⁷, A. Petrolini^{20,i}, M. Petruzzo²², E. Picatoste Olloqui³⁷,
 B. Pietrzyk⁴, T. Pilar⁴⁹, D. Pinci²⁶, A. Pistone²⁰, A. Piucci¹², S. Playfer⁵¹, M. Plo Casasus³⁸,
 T. Poikela³⁹, F. Polci⁸, A. Poluektov^{49,35}, I. Polyakov³², E. Polycarpo², A. Popov³⁶,
 D. Popov^{11,39}, B. Popovici³⁰, C. Potterat², E. Price⁴⁷, J.D. Price⁵³, J. Prisciandaro⁴⁰,
 A. Pritchard⁵³, C. Prouve⁴⁷, V. Pugatch⁴⁵, A. Puig Navarro⁴⁰, G. Punzi^{24,r}, W. Qian⁴,
 R. Quagliani^{7,47}, B. Rachwal²⁷, J.H. Rademacker⁴⁷, M. Rama²⁴, M.S. Rangel², I. Raniuk⁴⁴,
 N. Rauschmayr³⁹, G. Raven⁴³, F. Redi⁵⁴, S. Reichert⁵⁵, M.M. Reid⁴⁹, A.C. dos Reis¹,
 S. Ricciardi⁵⁰, S. Richards⁴⁷, M. Rihl³⁹, K. Rinnert⁵³, V. Rives Molina³⁷, P. Robbe^{7,39},
 A.B. Rodrigues¹, E. Rodrigues⁵⁵, J.A. Rodriguez Lopez⁶³, P. Rodriguez Perez⁵⁵, S. Roiser³⁹,

V. Romanovsky³⁶, A. Romero Vidal³⁸, J. W. Ronayne¹³, M. Rotondo²³, J. Rouvinet⁴⁰, T. Ruf³⁹, P. Ruiz Valls⁶⁷, J.J. Saborido Silva³⁸, N. Sagidova³¹, P. Sail⁵², B. Saitta^{16,e}, V. Salustino Guimaraes², C. Sanchez Mayordomo⁶⁷, B. Sanmartin Sedes³⁸, R. Santacesaria²⁶, C. Santamarina Rios³⁸, M. Santimaria¹⁹, E. Santovetti^{25,k}, A. Sarti^{19,l}, C. Satriano^{26,m}, A. Satta²⁵, D.M. Saunders⁴⁷, D. Savrina^{32,33}, S. Schael⁹, M. Schiller³⁹, H. Schindler³⁹, M. Schlupp¹⁰, M. Schmelling¹¹, T. Schmelzer¹⁰, B. Schmidt³⁹, O. Schneider⁴⁰, A. Schopper³⁹, M. Schubiger⁴⁰, M.-H. Schune⁷, R. Schwemmer³⁹, B. Sciascia¹⁹, A. Sciubba^{26,l}, A. Semennikov³², A. Sergi⁴⁶, N. Serra⁴¹, J. Serrano⁶, L. Sestini²³, P. Seyfert²¹, M. Shapkin³⁶, I. Shapoval^{17,44,f}, Y. Shcheglov³¹, T. Shears⁵³, L. Shekhtman³⁵, V. Shevchenko⁶⁵, A. Shires¹⁰, B.G. Siddi¹⁷, R. Silva Coutinho⁴¹, L. Silva de Oliveira², G. Simi^{23,r}, M. Sirendi⁴⁸, N. Skidmore⁴⁷, T. Skwarnicki⁶⁰, E. Smith^{56,50}, E. Smith⁵⁴, I.T. Smith⁵¹, J. Smith⁴⁸, M. Smith⁵⁵, H. Snoek⁴², M.D. Sokoloff^{58,39}, F.J.P. Soler⁵², F. Soomro⁴⁰, D. Souza⁴⁷, B. Souza De Paula², B. Spaan¹⁰, P. Spradlin⁵², S. Sridharan³⁹, F. Stagni³⁹, M. Stahl¹², S. Stahl³⁹, S. Stefkova⁵⁴, O. Steinkamp⁴¹, O. Stenyakin³⁶, S. Stevenson⁵⁶, S. Stoica³⁰, S. Stone⁶⁰, B. Storaci⁴¹, S. Stracka^{24,s}, M. Straticiu³⁰, U. Straumann⁴¹, L. Sun⁵⁸, W. Sutcliffe⁵⁴, K. Swientek²⁸, S. Swientek¹⁰, V. Syropoulos⁴³, M. Szczekowski²⁹, P. Szczypka^{40,39}, T. Szumlak²⁸, S. T'Jampens⁴, A. Tayduganov⁶, T. Tekampe¹⁰, M. Teklishyn⁷, G. Tellarini^{17,f}, F. Teubert³⁹, C. Thomas⁵⁶, E. Thomas³⁹, J. van Tilburg⁴², V. Tisserand⁴, M. Tobin⁴⁰, J. Todd⁵⁸, S. Tolk⁴³, L. Tomassetti^{17,f}, D. Tonelli³⁹, S. Topp-Joergensen⁵⁶, N. Torr⁵⁶, E. Tournefier⁴, S. Tourneur⁴⁰, K. Trabelsi⁴⁰, M.T. Tran⁴⁰, M. Tresch⁴¹, A. Trisovic³⁹, A. Tsaregorodtsev⁶, P. Tsopelas⁴², N. Tuning^{42,39}, A. Ukleja²⁹, A. Ustyuzhanin^{66,65}, U. Uwer¹², C. Vacca^{16,39,e}, V. Vagnoni¹⁵, G. Valenti¹⁵, A. Vallier⁷, R. Vazquez Gomez¹⁹, P. Vazquez Regueiro³⁸, C. Vázquez Sierra³⁸, S. Vecchi¹⁷, M. van Veghel⁴², J.J. Velthuis⁴⁷, M. Veltri^{18,g}, G. Veneziano⁴⁰, M. Vesterinen¹², B. Viaud⁷, D. Vieira², M. Vieites Diaz³⁸, X. Vilasis-Cardona^{37,o}, A. Vollhardt⁴¹, D. Volyanskyy¹¹, D. Voong⁴⁷, A. Vorobyev³¹, V. Vorobyev³⁵, C. Voß⁶⁴, J.A. de Vries⁴², R. Waldi⁶⁴, C. Wallace⁴⁹, R. Wallace¹³, J. Walsh²⁴, S. Wandernoth¹², J. Wang⁶⁰, D.R. Ward⁴⁸, N.K. Watson⁴⁶, D. Websdale⁵⁴, A. Weiden⁴¹, M. Whitehead⁴⁹, G. Wilkinson^{56,39}, M. Wilkinson⁶⁰, M. Williams³⁹, M.P. Williams⁴⁶, M. Williams⁵⁷, T. Williams⁴⁶, F.F. Wilson⁵⁰, J. Wimberley⁵⁹, J. Wishahi¹⁰, W. Wislicki²⁹, M. Witek²⁷, G. Wormser⁷, S.A. Wotton⁴⁸, S. Wright⁴⁸, K. Wyllie³⁹, Y. Xie⁶², Z. Xu⁴⁰, Z. Yang³, J. Yu⁶², X. Yuan³⁵, O. Yushchenko³⁶, M. Zangoli¹⁵, M. Zavertyaev^{11,b}, L. Zhang³, Y. Zhang³, A. Zhelezov¹², A. Zhokhov³², L. Zhong³, V. Zhukov⁹, S. Zucchelli¹⁵.

¹ Centro Brasileiro de Pesquisas Físicas (CBPF), Rio de Janeiro, Brazil

² Universidade Federal do Rio de Janeiro (UFRJ), Rio de Janeiro, Brazil

³ Center for High Energy Physics, Tsinghua University, Beijing, China

⁴ LAPP, Université Savoie Mont-Blanc, CNRS/IN2P3, Annecy-Le-Vieux, France

⁵ Clermont Université, Université Blaise Pascal, CNRS/IN2P3, LPC, Clermont-Ferrand, France

⁶ CPPM, Aix-Marseille Université, CNRS/IN2P3, Marseille, France

⁷ LAL, Université Paris-Sud, CNRS/IN2P3, Orsay, France

⁸ LPNHE, Université Pierre et Marie Curie, Université Paris Diderot, CNRS/IN2P3, Paris, France

⁹ I. Physikalisches Institut, RWTH Aachen University, Aachen, Germany

¹⁰ Fakultät Physik, Technische Universität Dortmund, Dortmund, Germany

¹¹ Max-Planck-Institut für Kernphysik (MPIK), Heidelberg, Germany

¹² Physikalisches Institut, Ruprecht-Karls-Universität Heidelberg, Heidelberg, Germany

¹³ School of Physics, University College Dublin, Dublin, Ireland

¹⁴ Sezione INFN di Bari, Bari, Italy

¹⁵ Sezione INFN di Bologna, Bologna, Italy

- ¹⁶ *Sezione INFN di Cagliari, Cagliari, Italy*
- ¹⁷ *Sezione INFN di Ferrara, Ferrara, Italy*
- ¹⁸ *Sezione INFN di Firenze, Firenze, Italy*
- ¹⁹ *Laboratori Nazionali dell'INFN di Frascati, Frascati, Italy*
- ²⁰ *Sezione INFN di Genova, Genova, Italy*
- ²¹ *Sezione INFN di Milano Bicocca, Milano, Italy*
- ²² *Sezione INFN di Milano, Milano, Italy*
- ²³ *Sezione INFN di Padova, Padova, Italy*
- ²⁴ *Sezione INFN di Pisa, Pisa, Italy*
- ²⁵ *Sezione INFN di Roma Tor Vergata, Roma, Italy*
- ²⁶ *Sezione INFN di Roma La Sapienza, Roma, Italy*
- ²⁷ *Henryk Niewodniczanski Institute of Nuclear Physics Polish Academy of Sciences, Kraków, Poland*
- ²⁸ *AGH - University of Science and Technology, Faculty of Physics and Applied Computer Science, Kraków, Poland*
- ²⁹ *National Center for Nuclear Research (NCBJ), Warsaw, Poland*
- ³⁰ *Horia Hulubei National Institute of Physics and Nuclear Engineering, Bucharest-Magurele, Romania*
- ³¹ *Petersburg Nuclear Physics Institute (PNPI), Gatchina, Russia*
- ³² *Institute of Theoretical and Experimental Physics (ITEP), Moscow, Russia*
- ³³ *Institute of Nuclear Physics, Moscow State University (SINP MSU), Moscow, Russia*
- ³⁴ *Institute for Nuclear Research of the Russian Academy of Sciences (INR RAN), Moscow, Russia*
- ³⁵ *Budker Institute of Nuclear Physics (SB RAS) and Novosibirsk State University, Novosibirsk, Russia*
- ³⁶ *Institute for High Energy Physics (IHEP), Protvino, Russia*
- ³⁷ *Universitat de Barcelona, Barcelona, Spain*
- ³⁸ *Universidad de Santiago de Compostela, Santiago de Compostela, Spain*
- ³⁹ *European Organization for Nuclear Research (CERN), Geneva, Switzerland*
- ⁴⁰ *Ecole Polytechnique Fédérale de Lausanne (EPFL), Lausanne, Switzerland*
- ⁴¹ *Physik-Institut, Universität Zürich, Zürich, Switzerland*
- ⁴² *Nikhef National Institute for Subatomic Physics, Amsterdam, The Netherlands*
- ⁴³ *Nikhef National Institute for Subatomic Physics and VU University Amsterdam, Amsterdam, The Netherlands*
- ⁴⁴ *NSC Kharkiv Institute of Physics and Technology (NSC KIPT), Kharkiv, Ukraine*
- ⁴⁵ *Institute for Nuclear Research of the National Academy of Sciences (KINR), Kyiv, Ukraine*
- ⁴⁶ *University of Birmingham, Birmingham, United Kingdom*
- ⁴⁷ *H.H. Wills Physics Laboratory, University of Bristol, Bristol, United Kingdom*
- ⁴⁸ *Cavendish Laboratory, University of Cambridge, Cambridge, United Kingdom*
- ⁴⁹ *Department of Physics, University of Warwick, Coventry, United Kingdom*
- ⁵⁰ *STFC Rutherford Appleton Laboratory, Didcot, United Kingdom*
- ⁵¹ *School of Physics and Astronomy, University of Edinburgh, Edinburgh, United Kingdom*
- ⁵² *School of Physics and Astronomy, University of Glasgow, Glasgow, United Kingdom*
- ⁵³ *Oliver Lodge Laboratory, University of Liverpool, Liverpool, United Kingdom*
- ⁵⁴ *Imperial College London, London, United Kingdom*
- ⁵⁵ *School of Physics and Astronomy, University of Manchester, Manchester, United Kingdom*
- ⁵⁶ *Department of Physics, University of Oxford, Oxford, United Kingdom*
- ⁵⁷ *Massachusetts Institute of Technology, Cambridge, MA, United States*
- ⁵⁸ *University of Cincinnati, Cincinnati, OH, United States*
- ⁵⁹ *University of Maryland, College Park, MD, United States*
- ⁶⁰ *Syracuse University, Syracuse, NY, United States*
- ⁶¹ *Pontifícia Universidade Católica do Rio de Janeiro (PUC-Rio), Rio de Janeiro, Brazil, associated to ²*
- ⁶² *Institute of Particle Physics, Central China Normal University, Wuhan, Hubei, China, associated to ³*
- ⁶³ *Departamento de Física, Universidad Nacional de Colombia, Bogota, Colombia, associated to ⁸*
- ⁶⁴ *Institut für Physik, Universität Rostock, Rostock, Germany, associated to ¹²*
- ⁶⁵ *National Research Centre Kurchatov Institute, Moscow, Russia, associated to ³²*

⁶⁶ *Yandex School of Data Analysis, Moscow, Russia, associated to* ³²

⁶⁷ *Instituto de Física Corpuscular (IFIC), Universitat de Valencia-CSIC, Valencia, Spain, associated to* ³⁷

⁶⁸ *Van Swinderen Institute, University of Groningen, Groningen, The Netherlands, associated to* ⁴²

^a *Universidade Federal do Triângulo Mineiro (UFTM), Uberaba-MG, Brazil*

^b *P.N. Lebedev Physical Institute, Russian Academy of Science (LPI RAS), Moscow, Russia*

^c *Università di Bari, Bari, Italy*

^d *Università di Bologna, Bologna, Italy*

^e *Università di Cagliari, Cagliari, Italy*

^f *Università di Ferrara, Ferrara, Italy*

^g *Università di Urbino, Urbino, Italy*

^h *Università di Modena e Reggio Emilia, Modena, Italy*

ⁱ *Università di Genova, Genova, Italy*

^j *Università di Milano Bicocca, Milano, Italy*

^k *Università di Roma Tor Vergata, Roma, Italy*

^l *Università di Roma La Sapienza, Roma, Italy*

^m *Università della Basilicata, Potenza, Italy*

ⁿ *AGH - University of Science and Technology, Faculty of Computer Science, Electronics and Telecommunications, Kraków, Poland*

^o *LIFAELS, La Salle, Universitat Ramon Llull, Barcelona, Spain*

^p *Hanoi University of Science, Hanoi, Viet Nam*

^q *Università di Padova, Padova, Italy*

^r *Università di Pisa, Pisa, Italy*

^s *Scuola Normale Superiore, Pisa, Italy*

^t *Università degli Studi di Milano, Milano, Italy*

[†] *Deceased*